

Even-order high-harmonic generation from solids in velocity gauge

Jiayuan Cao (曹佳媛)^{1,2}, Na Li (李娜)¹, Ya Bai (白亚)^{1*}, Peng Liu (刘鹏)^{1,2**}, and Ruxin Li (李儒新)¹

¹State Key Laboratory of High Field Laser Physics and CAS Center for Excellence in Ultra-Intense Laser Science, Shanghai Institute of Optics and Fine Mechanics, Chinese Academy of Sciences, Shanghai 201800, China

²Center of Materials Science and Optoelectronics Engineering, University of Chinese Academy of Sciences, Beijing 100049, China

*Corresponding author: pijbear@siom.ac.cn

**Corresponding author: peng@siom.ac.cn

Received August 20, 2020 | Accepted October 19, 2020 | Posted Online January 13, 2021

We present a velocity-gauge model for the generation of even-order high harmonics, and reveal that the even-order harmonics originate from the multiple-step transitions among the energy bands in momentum space, while the odd-order harmonics are mainly from direct transitions. The lower valence band is found vital for the generation of even harmonics. Relative intensity of even-order harmonics versus the odd orders is calculated and shows a growing trend as the laser field amplitude increases.

Keywords: solid high-harmonic generation; inversion asymmetry; even-order harmonics.

DOI: [10.3788/COL202119.043201](https://doi.org/10.3788/COL202119.043201)

1. Introduction

High-harmonic generation (HHG) in the gas phase^[1–3] has long been studied as a coherent soft X-ray radiation source with an extremely short pulse width^[4–6]. Its ability to probe the molecular structure^[7,8] and ultrafast electron dynamics^[9–11] has also been proved. Recently, HHG from solid state materials has attracted much attention^[12,13], as it provides an opportunity to probe electron dynamics in solid states and a potential to produce attosecond pulses with an enhanced yield^[14–24].

Because of the complexity of solid materials, HHG shows a variety of new phenomena and corresponding mechanisms. Especially, even-order harmonics are generated by breaking the inversion symmetry of the system^[16,17,25,26]. From a single crystal of gallium selenide (GaSe), even-order harmonics are produced with a comparable yield as the odd orders, which are attributed to the interference between multiple interband transitions^[16]. It has also been proved that the transition dipole phase (TDP) is a necessity for modeling HHG, with which even-order harmonics can be produced by only considering a direct two-band transition^[25,27]. Recently, the Berry connection is found crucial to calculate a physical HHG spectrum that includes even-order harmonics^[28,29]. It is noted that all available descriptions of even-order harmonic generation rely on the length gauge, and multiple parameters increase the complexity to interpret experimental observations.

As an electromagnetic gauge to describe the light field under dipole approximation, the velocity gauge preserves the

translational symmetry of the crystal and decouples electron dynamics at each crystal momentum (k) point^[30], which can be advantageous to study laser–solid interaction. In this work, we study the generation of even-order harmonics by calculating the high-harmonic spectrum from an inversion-asymmetric one-dimensional periodic potential. Under the picture of velocity gauge, we proved that the even-order harmonics only originate from the multiple-step transition, while the odd orders are mainly from the direct one. The lower valence band is found crucial to the generation of even-order harmonics, which differs from the inversion-symmetric case. We find the relative intensity of even versus odd harmonics increases over pump laser intensity, which results from the growing hole population in the lower valence band.

2. Method

We model the inversion-asymmetric crystal structure as a one-dimensional chain constituted by three kinds of atoms equally spaced [Fig. 1(a)]. The Coulomb potential of each atom is treated as a localized potential well^[31,32]. The total periodic potential is given by

$$V(x) = \sum_R \sum_{i=A,B,C} V_i [1 + \tanh(x - x_{i,R})][1 - \tanh(x - x_{i,R})], \quad (1)$$

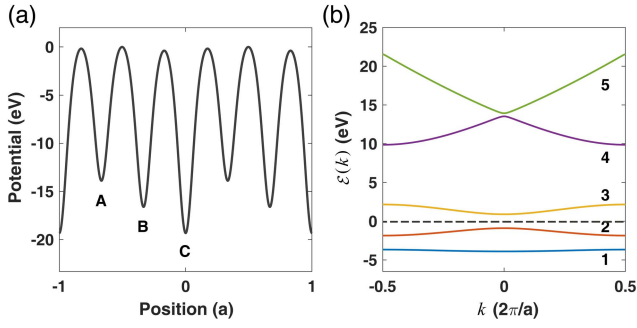


Fig. 1. (a) Periodic potential used for the calculation. Each crystal lattice includes three different atomic centers, namely, A, B, and C. (b) The corresponding band structure [first five bands]. Band indices are shown on the right. The gray dashed line indicates the Fermi level.

in which $V_A = 0.6$, $V_B = 0.7$, and $V_C = 0.8$ in atomic units (a.u.). Atomic centers are separated by $1/3$ of the lattice constant $a = x_{i,R} - x_{i,R-1} = 12$ a.u. Note that three different atoms in each lattice are the simplest asymmetric case for equally spaced atoms. We calculate the Bloch functions as eigenfunctions of the field-free Hamiltonian, and the energies of the first five bands ($\varepsilon_{n,k}$, $n = 1, 2, 3, 4, 5$) are shown in Fig. 1(b).

Under dipole approximation, the multiple-electron dynamics of the system is calculated using the semiconductor Bloch equation (SBE) in the velocity gauge with a phenomenological relaxation rate^[29]:

$$\begin{aligned} \frac{\partial}{\partial t} P_{n,n'}(k,t) &= -i(\tilde{\varepsilon}_{n,k} - \tilde{\varepsilon}_{n',k} - i/T_2)P_{n,n'}(k,t) \\ &+ iA(t)[\rho_n(k,t) - \rho_{n'}(k,t)]p_{n,n'}(k) \\ &- iA(t)\sum_m [P_{m,n'}(k,t)p_{n,m}(k) - P_{n,m}(k,t)p_{m,n'}(k)], \quad (2) \end{aligned}$$

$$\frac{\partial}{\partial t} \rho_n(k,t) = -\rho_n(k,t)/T_1 - 2A(t)\text{Im}\left[\sum_m P_{n,m}(k,t)p_{m,n}(k)\right], \quad (3)$$

where $p_{n,n'}(k) = -i\langle\phi_{n,k}|\nabla_k|\phi_{n',k}\rangle$ is the transition matrix element calculated from Bloch functions, $P_{n,n'}(k,t)$ is the microscopic polarization, $\rho_n(k,t)$ is the electron population, and $\tilde{\varepsilon}_{n,k}$ is the modified band energy, $\tilde{\varepsilon}_{n,k} = \varepsilon_{n,k} + A(t)p_{n,n}(k)$.

In our calculation, the laser pulse has an electric field $E(t) = E_L \cos^4(t/\tau) \cos(2\omega_L t)$ with a wavelength of $\lambda_L = 2\pi c/\omega_L = 4 \mu\text{m}$ and pulse duration of $\tau = 63$ fs. The relaxation times T_1 and T_2 are set to be 7 fs and 1.1 fs, respectively^[16]. For initial conditions, we set $\rho_1(k,0) = \rho_2(k,0) = 1$, while other $\rho_n(k,0)$ and $P_{n,n'}(k,0)$ are all zero [see the Fermi level shown in Fig. 1(b)]^[31,33,34].

After solving Eqs. (2) and (3), we calculate the electric current by

$$j(t) \propto \sum_{k,n,n'} P_{n,n'}^*(k,t)p_{n,n'}(k) + \sum_{k,n} \rho_n(k,t)[p_{n,n}(k) + A(t)]. \quad (4)$$

The high-harmonic spectrum is given by

$$S(\omega) \propto \omega^2 |j(\omega)|^2. \quad (5)$$

3. Results and Discussion

The high-harmonic spectrum at the pump laser field amplitude of $E_L = 2.2$ V/nm is shown in Fig. 2(a). Five bands in total have been involved in the calculation. The convergence of results in this spectrum range has been checked for up to 10 bands. The spectrum contains both odd and even orders. While being generally weaker than adjacent odd orders, a plateau of even-order harmonics, ranging from the 6th to 14th order, is clearly shown in Fig. 2(a). The abrupt increase of harmonic intensity between the 4th and 6th order coincides with the first Van Hove singularity point shown by the joint density of states (JDos) [Fig. 2(b)]. For orders higher than the 14th, the intensity of even-order harmonics begins to decrease with increasing order. Such pattern complies with the interband mechanism^[20,35].

To determine the transition path that leads to the generation of even-order harmonics, we turn off the sequential transition by setting $p_{n,n'} = 0$ for all $|n - n'| > 1$ in the calculation. As a result, one can see the even-order harmonics disappear completely in the spectrum (Fig. 3), which indicates that they originate from the multiple-band mechanism. The spectrum of odd harmonics also slightly changes in Fig. 3, which implies minor contributions from sequential transitions as well. The calculation is done

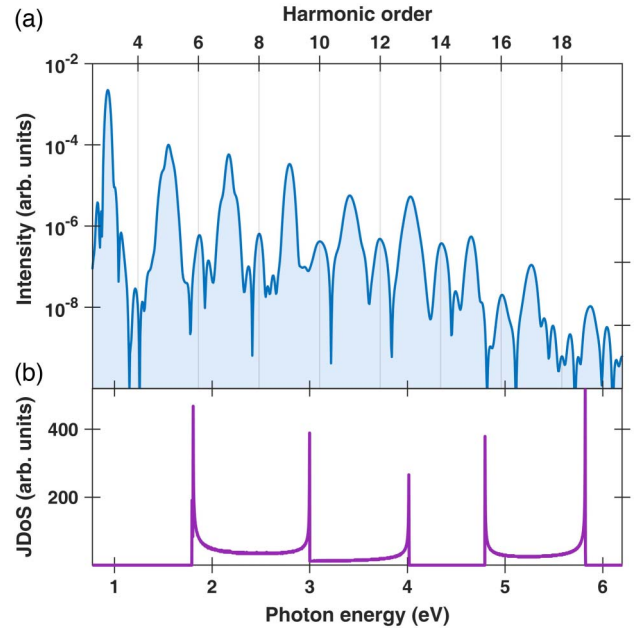


Fig. 2. (a) Calculated high-harmonic spectrum. (b) The JDos of the system.

under several laser field strengths (0.8–2.4 V/nm), and the result stays the same.

It is noted that a direct two-band transition can produce even-order harmonics in the length gauge, in which it is crucial that the TDP be included^[25,27]. In our calculation, since we have obtained the Bloch functions, the phase of the transition dipole is included. But, the spectrum produced by forbidding all sequential transitions in Fig. 3 does not include even orders. This is because in the velocity gauge, the two-band transition with the transition matrix element phase does not contribute to the even-order harmonics.

To prove the above statement analytically, we reduce Eq. (2) into a two-band case:

$$\frac{\partial}{\partial t} P_{c,v}(k,t) = -i(\tilde{\epsilon}_{c,k} - \tilde{\epsilon}_{v,k} - i/T_2)P_{c,v}(k,t) + iA(t)[1 - \rho(k,t)]p_{c,v}(k). \quad (6)$$

Note that in velocity-gauge SBE [Eqs. (2), (3), and (6)] the system evolution at each k is completely decoupled. Following Keldysh's approach^[3,36,37], Eq. (6) can be written as

$$P_{c,v}(k,t) = i \int_{-\infty}^t [1 - \rho(k,t)]A(\tau)p_{c,v}(k)d\tau e^{iS} e^{-\frac{t-\tau}{T_2}}, \quad (7)$$

where S is the dynamical phase, $S = -\int_{\tau}^t \tilde{\epsilon}_{n,k} dt'$.

Applying Eq. (4), the corresponding current is

$$j(t) \propto i \sum_k p_{c,v}^*(k) \int_{-\infty}^t [1 - \rho(k,t)]A(\tau)p_{c,v}(k)d\tau e^{iS} e^{-\frac{t-\tau}{T_2}} + c.c. \quad (8)$$

In Eq. (8), the complex phase of $p_{c,v}$ inside and outside the integral sign cancels out and does not affect the result current. Following a similar routine, one can prove that the current generated by band population $\rho_n(k,t)$ is not affected by the phase of $p_{c,v}$ either. Since, in such one-dimensional two-band systems,

the asymmetry of the material is encoded in the phase of $p_{c,v}$ (which is linked to TDP by a phase shift of $\pi/2$)^[25], the irrelevance of the phase of $p_{c,v}$ means the asymmetry of the material is omitted in the high-harmonic current, and thus no even-order harmonics can be generated.

We want to clarify that our conclusion does not conflict that of Ref. [25], which finds that the TDP dominates the even-order harmonic generation process in ZnO, because the electromagnetic gauges we use are different. Under electromagnetic-gauge transformation, the corresponding electron transition path is known to be different^[38].

As the generation of even-order harmonics results from sequential transitions, we further specify the role of the individual band. In the inversion-symmetric system with a similar band structure^[33], it has been found that the lower valence band plays a negligible role in HHG. We test the applicability of the finding in our system by forbidding all transitions involving band 1 and compare the spectrum with the real one (Fig. 4). The result shows that when band 1 is excluded it does not affect much of the odd harmonics, which agrees with the previous finding. Meanwhile, nearly most of the even-order harmonics disappeared, which distinctively differs from the symmetric case. We have checked the result under several laser field strengths (0.8–2.4 V/nm). The key role of band 1 in even-order harmonic generation can be understood, as it includes the most bounded states of the system, and thus is sensitive to the asymmetry of the periodic potential.

We then calculate the laser field dependence of the yield of even-order harmonics on the odd orders. The result is shown in Fig. 5(a). At the field strength of $E_L = 1.0$ V/nm, the even-order harmonics are weaker than adjacent odd harmonics by two to three orders of magnitude. As the laser field increases to $E_L = 2.4$ V/nm, the yield of the 12th and 14th becomes of the same order of magnitude as adjacent odd orders. To show the dependence more clearly, we calculate the ratio between the even-order harmonics and their neighboring two odd orders, $I_{2s}/(I_{2s+1}I_{2s-1})^{0.5}$. As shown in Fig. 5(b), the calculated ratio has an increasing trend and minor oscillation.

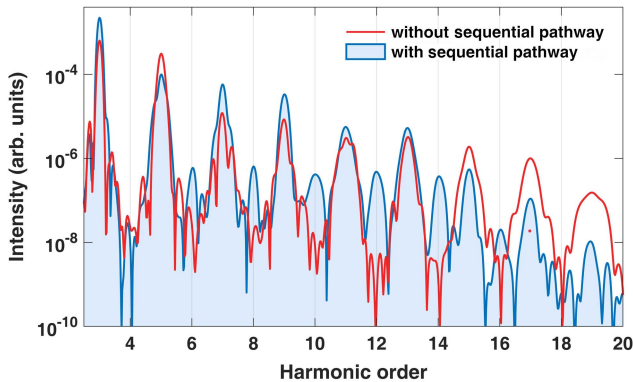


Fig. 3. Comparison between the harmonic spectra obtained by allowing (blue line) and forbidding (red line) multiple-band transitions. Initial electron state and laser parameters are the same as in Fig. 2(a).

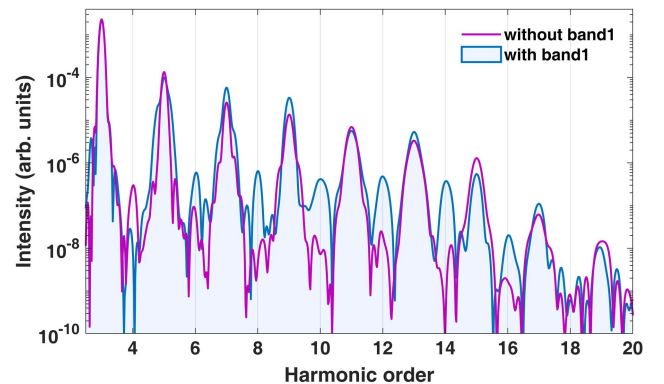


Fig. 4. Comparison of high-harmonic spectra calculated with (blue line) and without (pink line) transitions involving band 1.

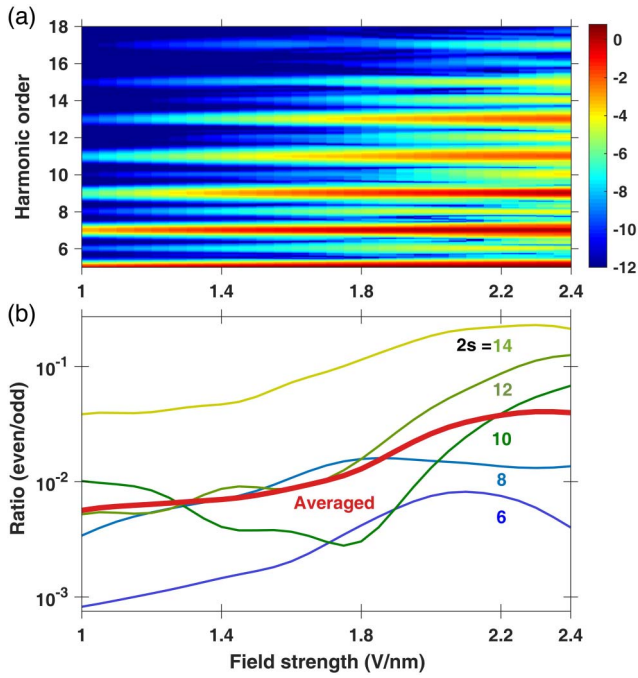


Fig. 5. Laser field dependence of the high harmonics. (a) Calculated high-harmonic spectra between the 5th and 18th harmonic order. (b) The even/odd ratio of the 6th–14th harmonics. Red solid line shows the averaged ratio.

Our analysis above shows that the even-order harmonics are generated by sequential transitions involving band 1, while the odd orders are generated mostly from direct transitions. Next, we will show how the two processes depend differently on the increase of the laser field. A schematic diagram is shown in Fig. 6. For the odd harmonics, the harmonic intensity is determined by the probability of direct transition $m \rightarrow n$, $O_{m \rightarrow n}$, while for the even-order harmonics, by the probability of sequential transition $1 \rightarrow m \rightarrow n$, $O_{1 \rightarrow m \rightarrow n}$. Note that the only difference of the two transitions is the involvement of band 1. Under low laser amplitude, band 1 is hardly involved with being tightly bounded. Under higher laser amplitude, the involvement of band 1 is increased, which gives rise to the ratio between the probabilities of the two transitions $O_{1 \rightarrow m \rightarrow n}/O_{m \rightarrow n}$. This explains the increasing trend of relative yield of even-order harmonics. Since the yield of high harmonics also depends on

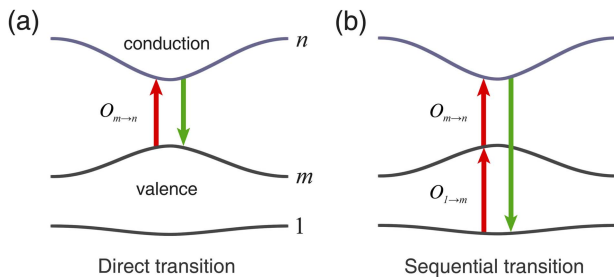


Fig. 6. Schematic diagram of the (a) direct transition and (b) sequential transition processes. Number and letters on the right of (a) are band indices.

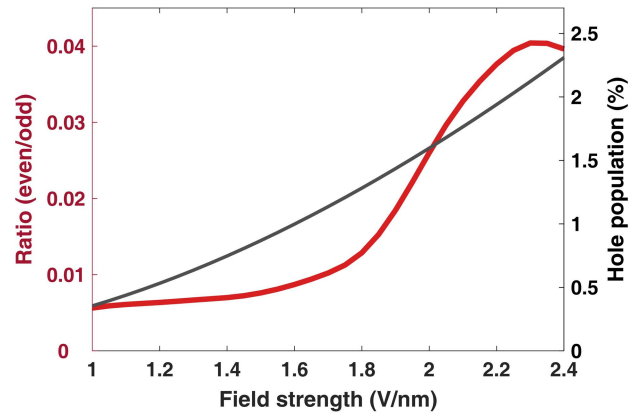


Fig. 7. Comparison between the hole population in band 1 and the averaged ratio between even- and odd-order harmonics as functions of laser field strength.

dynamical phase^[37], which changes as well with pump intensity, the relative intensity of even-order harmonics as a function of laser field is not monotonous, as is shown in Fig. 5(b). But, as we average the ratio of different even orders, the increasing trend is clear.

We check the above explanation by comparing the hole population in band 1, $1 - \rho_1$, with averaged even/odd ratios. As shown in Fig. 7, the two curves roughly coincide with one another, which supports the validity of our explanation.

As the phenomenological relaxation rate in Eqs. (2) and (3) can suppress some electron trajectories for HHG^[39], the numerical results are quantitatively dependent on the relaxation rate used in our calculation. But, as even and odd harmonics mainly come from different electron transition paths, one can imagine that their yield should depend differently on laser parameters. Though our analysis is based on velocity gauge, considering gauge freedom, analysis including the TDP and Berry connection in length gauge^[25,28,29] should lead to the same result. In real systems, the second harmonics generated from the material front surface can also drive the electron and lead to the generation of even-order harmonics^[26]. This might be the reason that in some experimental results even and odd harmonics have similar laser intensity dependence^[16,40]. It has been shown that with reflection geometry such nonlinear propagation effects can be suppressed^[41].

4. Conclusion

In conclusion, we calculated the high-harmonics spectra from an inversion-asymmetric one-dimensional periodic potential. The result is understood in velocity gauge, where the even-order harmonics contribute solely to sequential transitions, and the odd harmonics mostly to direct transitions. The vital role of the lower valence band in even-order harmonic generation is found in our result. As the involvement of the lower valence band requires high laser intensity, the yield of even-order harmonics increases more rapidly with the laser field than

odd-order harmonics. The difference between the laser intensity dependence of even and adjacent odd harmonics should be independent of gauge and can be examined by experiments free from propagation effects. Our work offers an alternative perspective to study the interplay between the intense laser field and inversion-asymmetric solids. As even-order harmonics are linked only to sequential transition processes, our work implies a way to resolve the electron motion using high-harmonic spectroscopy.

Acknowledgement

This work was supported by the National Natural Science Foundation of China (NSFC) (Nos. 11127901, 11134010, 61221064, and 61405222) and the Strategic Priority Research Program of Chinese Academy of Sciences (CAS) (No. XDB16000000).

References

1. A. McPherson, G. Gibson, H. Jara, U. Johann, T. S. Luk, I. A. McIntyre, K. Boyer, and C. K. Rhodes, "Studies of multiphoton production of vacuum-ultraviolet radiation in the rare gases," *J. Opt. Soc. Am. B* **4**, 595 (1987).
2. J. L. Krause, K. J. Schafer, and K. C. Kulander, "High-order harmonic generation from atoms and ions in the high intensity regime," *Phys. Rev. Lett.* **68**, 3535 (1992).
3. M. Lewenstein, Ph. Balcou, M. Yu. Ivanov, A. L'Huillier, and P. B. Corkum, "Theory of high-harmonic generation by low-frequency laser fields," *Phys. Rev. A* **49**, 2117 (1994).
4. P. M. Paul, E. S. Toma, P. Breger, G. Mullot, F. Augé, Ph. Balcou, H. G. Muller, and P. Agostini, "Observation of a train of attosecond pulses from high harmonic generation," *Science* **292**, 1689 (2001).
5. G. Sansone, E. Benedetti, F. Calegari, C. Vozzi, L. Avaldi, R. Flammini, L. Poletto, P. Villoresi, C. Altucci, R. Velotta, S. Stagira, S. De Silvestri, and M. Nisoli, "Isolated single-cycle attosecond pulses," *Science* **314**, 443 (2006).
6. F. Krausz and M. Ivanov, "Attosecond physics," *Rev. Mod. Phys.* **81**, 163 (2009).
7. J. Itatani, J. Levesque, D. Zeidler, H. Niikura, H. Pépin, J. C. Kieffer, P. B. Corkum, and D. M. Villeneuve, "Tomographic imaging of molecular orbitals," *Nature* **432**, 867 (2004).
8. C. Vozzi, M. Negro, F. Calegari, G. Sansone, M. Nisoli, S. De Silvestri, and S. Stagira, "Generalized molecular orbital tomography," *Nat. Phys.* **7**, 822 (2011).
9. T. Kanai, S. Minemoto, and H. Sakai, "Quantum interference during high-order harmonic generation from aligned molecules," *Nature* **435**, 470 (2005).
10. B. K. McFarland, J. P. Farrell, P. H. Bucksbaum, and M. Guhr, "High harmonic generation from multiple orbitals in N_2 ," *Science* **322**, 1232 (2008).
11. O. Smirnova, Y. Mairesse, S. Patchkovskii, N. Dudovich, D. Villeneuve, P. Corkum, and M. Yu. Ivanov, "High harmonic interferometry of multi-electron dynamics in molecules," *Nature* **460**, 972 (2009).
12. S. Ghimire, A. D. DiChiara, E. Sistrunk, P. Agostini, L. F. DiMauro, and D. A. Reis, "Observation of high-order harmonic generation in a bulk crystal," *Nat. Phys.* **7**, 138 (2011).
13. S. Ghimire and D. A. Reis, "High-harmonic generation from solids," *Nat. Phys.* **15**, 10 (2019).
14. O. Schubert, M. Hohenleutner, F. Langer, B. Urbanek, C. Lange, U. Huttner, D. Golde, T. Meier, M. Kira, S. W. Koch, and R. Huber, "Sub-cycle control of terahertz high-harmonic generation by dynamical Bloch oscillations," *Nat. Photon.* **8**, 119 (2014).
15. G. Vampa, T. J. Hammond, N. Thiré, B. E. Schmidt, F. Légaré, C. R. McDonald, T. Brabec, and P. B. Corkum, "Linking high harmonics from gases and solids," *Nature* **522**, 462 (2015).
16. M. Hohenleutner, F. Langer, O. Schubert, M. Knorr, U. Huttner, S. W. Koch, M. Kira, and R. Huber, "Real-time observation of interfering crystal electrons in high-harmonic generation," *Nature* **523**, 572 (2015).
17. H. Liu, Y. Li, Y. S. You, S. Ghimire, T. F. Heinz, and D. A. Reis, "High-harmonic generation from an atomically thin semiconductor," *Nat. Phys.* **13**, 262 (2017).
18. Y. W. Kim, T.-J. Shao, H. Kim, S. Han, S. Kim, M. Ciappina, X.-B. Bian, and S.-W. Kim, "Spectral interference in high harmonic generation from solids," *ACS Photon.* **6**, 851 (2019).
19. L.-J. Lü and X.-B. Bian, "Ultrafast intraband electron dynamics of preexcited SiO_2 ," *Opt. Express* **28**, 13432 (2020).
20. N. Yoshikawa, K. Nagai, K. Uchida, Y. Takaguchi, S. Sasaki, Y. Miyata, and K. Tanaka, "Interband resonant high-harmonic generation by valley polarized electron-hole pairs," *Nat. Commun.* **10**, 3709 (2019).
21. T. T. Luu, M. Garg, S. Yu. Kruchinin, A. Moulet, M. Th. Hassan, and E. Goulielmakis, "Extreme ultraviolet high-harmonic spectroscopy of solids," *Nature* **521**, 498 (2015).
22. M. Garg, M. Zhan, T. T. Luu, H. Lakhotia, T. Klostermann, A. Guggenmos, and E. Goulielmakis, "Multi-petahertz electronic metrology," *Nature* **538**, 359 (2016).
23. H. Kim, S. Han, Y. W. Kim, S. Kim, and S.-W. Kim, "Generation of coherent extreme-ultraviolet radiation from bulk sapphire crystal," *ACS Photon.* **4**, 1627 (2017).
24. L. Li, P. Lan, X. Zhu, T. Huang, Q. Zhang, M. Lein, and P. Lu, "Reciprocal-space-trajectory perspective on high-harmonic generation in solids," *Phys. Rev. Lett.* **122**, 193901 (2019).
25. S. Jiang, J. Chen, H. Wei, C. Yu, R. Lu, and C. D. Lin, "Role of the transition dipole amplitude and phase on the generation of odd and even high-order harmonics in crystals," *Phys. Rev. Lett.* **120**, 253201 (2018).
26. A. A. Lanin, E. A. Stepanov, A. B. Fedotov, and A. M. Zheltikov, "Mapping the electron band structure by intraband high-harmonic generation in solids," *Optica* **4**, 516 (2017).
27. S. Jiang, H. Wei, J. Chen, C. Yu, R. Lu, and C. D. Lin, "Effect of transition dipole phase on high-order-harmonic generation in solid materials," *Phys. Rev. A* **96**, 053850 (2017).
28. J. Li, X. Zhang, S. Fu, Y. Feng, B. Hu, and H. Du, "Phase invariance of the semiconductor Bloch equations," *Phys. Rev. A* **100**, 043404 (2019).
29. L. Yue and M. B. Gaarde, "Structure gauges and laser gauges for the semiconductor Bloch equations in high-order harmonic generation in solids," *Phys. Rev. A* **101**, 053411 (2020).
30. T. Tamaya, A. Ishikawa, T. Ogawa, and K. Tanaka, "Adiabatic mechanisms of higher-order harmonic generation in solid-state materials under high-intensity electric fields," *Phys. Rev. Lett.* **116**, 016601 (2016).
31. P. G. Hawkins, M. Yu. Ivanov, and V. S. Yakovlev, "Effect of multiple conduction bands on high-harmonic emission from dielectrics," *Phys. Rev. A* **91**, 013405 (2015).
32. M. Korbman, S. Yu Kruchinin, and V. S. Yakovlev, "Quantum beats in the polarization response of a dielectric to intense few-cycle laser pulses," *New J. Phys.* **15**, 013006 (2013).
33. M. Wu, S. Ghimire, D. A. Reis, K. J. Schafer, and M. B. Gaarde, "High-harmonic generation from Bloch electrons in solids," *Phys. Rev. A* **91**, 043839 (2015).
34. T. Ikemachi, Y. Shinohara, T. Sato, J. Yumoto, M. Kuwata-Gonokami, and K. L. Ishikawa, "Trajectory analysis of high-order-harmonic generation from periodic crystals," *Phys. Rev. A* **95**, 043416 (2017).
35. A. J. Uzan, G. Orenstein, Á. Jiménez-Galán, C. McDonald, R. E. F. Silva, B. D. Bruner, N. D. Klimkin, V. Blanchet, T. Arusi-Parpar, M. Krüger, A. N. Rubtsov, O. Smirnova, M. Ivanov, B. Yan, T. Brabec, and N. Dudovich, "Attosecond spectral singularities in solid-state high-harmonic generation," *Nat. Photon.* **14**, 183 (2020).
36. L. Keldysh, "Ionization in field of a strong electromagnetic wave," *Sov. Phys. JETP* **20**, 1307 (1965).
37. G. Vampa, C. R. McDonald, G. Orlando, D. D. Klug, P. B. Corkum, and T. Brabec, "Theoretical analysis of high-harmonic generation in solids," *Phys. Rev. Lett.* **113**, 073901 (2014).

38. P. Földi, "Gauge invariance and interpretation of interband and intraband processes in high-order harmonic generation from bulk solids," *Phys. Rev. B* **96**, 035112 (2017).
39. G. Vampa, C. R. McDonald, G. Orlando, P. B. Corkum, and T. Brabec, "Semiclassical analysis of high harmonic generation in bulk crystals," *Phys. Rev. B* **91**, 064302 (2015).
40. F. Langer, M. Hohenleutner, U. Huttner, S. W. Koch, M. Kira, and R. Huber, "Symmetry-controlled temporal structure of high-harmonic carrier fields from a bulk crystal," *Nat. Photon.* **11**, 227 (2017).
41. P. Xia, C. Kim, F. Lu, T. Kanai, H. Akiyama, J. Itatani, and N. Ishii, "Nonlinear propagation effects in high harmonic generation in reflection and transmission from gallium arsenide," *Opt. Express* **26**, 29393 (2018).